Holographic Three-Dimensional Computer-Aided Imaging

Joseph Rosen and David Abookasis
Ben-Gurion University of the Negev,
Department of Electrical and Computer Engineering
P. O. Box 653, Beer-Sheva 84105, Israel

ABSTRACT

Recent developments in a new method of holographic computer-aided imaging are reviewed. The proposed hologram is computed from angular viewpoints of the observed three-dimensional scene. The recorded data are processed to yield a two-dimensional computer-generated hologram. When this hologram is illuminated properly, a three-dimensional image of the scene is reconstructed.

Keywords: Holography, 3-D images, conventional camera, stereograms, 3-D display, computer generated hologram

1. INTRODUCTION

Current approaches to displaying three-dimensional (3-D) images can be classified into several main types: stereoscopic display,[1] volumetric system,[2] integral photography[3] (also known as integral imaging), and holography.[4] Each of these technologies has particular advantages and disadvantages. However, holography seems to be a more attractive method of displaying 3-D images than others because a single hologram is capable of creating the most authentic illusion of observing volumetric objects by the naked eye. Holographic technology supplies high-quality images and accurate depth cues viewed by human eyes without any special observation devices. Since the invention of the hologram more than 50 years ago,[5] holographic recording of real objects has been performed by wave interference. In general, interference between optical waves demands relatively intense light with a high degree of coherence between the involved beams. The optical system must be very stable, since a very slight movement can destroy the interference fringes, which contain both intensity and phase information. These requirements have prevented hologram recorders from becoming as widely used for outdoor photography as conventional cameras. A possible solution to these limitations is obtained by the techniques of holographic stereograms[6,7] (also known as multiplex holograms[8,9]). However, optical interference is also involved in recording of holographic stereograms, although it is off-line interference. However, unlike ordinary holograms,[5,10] holographic stereograms do not reconstruct the true wave front that is diffracted from an object when this object is coherently illuminated. The reconstructed wave front from a holographic stereogram is composed of a set of discrete patches; each patch contains a different perspective projection of the object. Because of the discontinuity between those patches, the imitation of the observed reality cannot be complete.

A partial solution for these limitations might be using computer-generated holograms (CGHs).[11,12] The objects to be constructed by the CGH can be represented in the computer by mathematical or graphical descriptions, or by their spatial samples. The physical interference between light waves is replaced by mathematical computation. However, synthesizing CGHs of 3-D images is usually a heavy computational task. This is because one needs to superpose the mathematical contributions of many waves originating from many points on the objects, when not all of them are located at the same distance from the hologram plane.

Many algorithms for synthesizing CGHs for 3-D imaging have been proposed in the past three decades. The choice among the various algorithms depends on different factors such as computation time, the hologram applications, and image characteristics.[13] In the early days of the CGH, Waters[14] designed a CGH based on the assumption that any object is constructed from many independent light scatterers, each of which is considered as a point source of a parabolic wave front. The superposition of all these complex amplitudes yields the desired complex amplitude distribution on the hologram plane. The depth information is retrievable from continuous parallax and from focusing on different transverse planes through the volume (accommodation effect). The difficulty of this technique comes from the long computation time necessary to superpose waves coming from large number of object points. Ichioka *et al.*[15] reduced the computation time using the ''ping pong'' algorithm. A method involving the acquisition of objects from different points of view was suggested by Yatagai.[16] His study followed an earlier pioneer work of George and McCrickerd,[17] who had first implemented the technique of the holographic stereogram. Yatagai's hologram has been composed of several Fourier

Current Research on Image Processing for 3D Information Displays,
edited by Vladimir V. Petrov, Proceedings of SPIE Vol. 5821
(SPIE, Bellingham, WA, 2005) · 0277-786X/05/$15 · doi: 10.1117/12.612118

holograms of perspective projections of different 3-D objects. In about the same years Yaroslavskii and Merzlyakov[18] also implemented the idea of stereoscopic technique in CGHs. When a viewer looks through such a composite hologram, each of his eyes sees a different perspective of the object, and a 3-D display is obtained through the stereoscopic effect. However, the quality of the image cannot be optimal because of the discontinuity between different projections. In another study Frère *et al.*[19] demonstrated a CGH of 3-D objects composed of finite line segments. As a result of several conditions and restrictions imposed on their reconstruction procedure, Leseberg and Frère[20] later were able to present an improvement of their method in which objects were composed of tilted and shifted planar segments. Tommasi and Bianco[21] proposed to generate an off-axis hologram of tilted and shifted surfaces in the spatial-frequency domain by using translation and rotation transformations of angular spectra. This frequency approach permits the use of the fast Fourier transform algorithm, which decreases the computation time and makes it possible to consider any position of the planes in space. In these last two methods it is necessary to model the object as a series of rotated and translated planes. Lucente[22] invented a more general method called diffraction-specific computation. This method is based on quantizing the space and the spatial frequency of the CGH. In contrast to conventional computation, diffraction-specific computation considers only the diffraction that occurs during the reconstruction of the holographic image. Thus the algorithm permits a trade-off between image quality and computational speed. Adopting Lucente's algorithm, Cameron *et al.*[23] developed a modified version of the algorithm called diffraction specific 1. In this algorithm they have used multiple plane waves to approximate the spherical wave that emanates from a given point in image-volume space. This gives an approximation of the accommodation depth cue. As a result, the human visual system gets the impression of a real point existing in space.

In this chapter, we review recently proposed method of holographic computer-aided imaging[24,25]. Generally in this method, a hologram is computed from a set of angular projections of the observed 3-D object, recorded by a conventional digital camera. The recorded data are numerically processed to yield a two-dimensional complex function, which is then encoded as a computer-generated hologram. When this hologram is illuminated by a plane wave, a 3-D real image of the object is reconstructed. The main feature of this hologram is that its transparency values are identical to a Fourier hologram recorded by an interference between two laser beams. It is important to note that this hologram is not related to the well-known multiplex or stereoscopic holograms. The main advantage of this technique is that, although objects in the scene are recorded by a conventional digital camera without wave interference, the process yields a hologram of the observed scene with a 3-D nature.

Following the presentation of the basic hologram, we describe different configurations of scanning the scene. The two main examples are, on one hand, a hologram computed from a set of different viewpoints along a horizontal arc around the observed object[24]. On the other hand, using two-dimensional (2-D) array of observation points enables us to capture the scene from horizontal as well as vertical points of view, and thus such a technique yields a different type of hologram.[25]

2. FOURIER – IMAGE HOLOGRAM OF 3-D SCENE

With the first type of hologram, we propose a process of recording a CGH of a real-world 3-D object under conditions of incoherent white illumination. Yet the true wave front diffracted from the object, when it is coherently illuminated, can be reconstructed from the proposed hologram. In other words, after a process of recording the scene under incoherent illumination and digital computing, we get a 2-D complex function. This function is equal to the complex amplitude of coherent light diffracted from the same object and propagates through a particular optical system described below. Thus apparently we succeed in recording the complex amplitude of some wave front without beam interference. It should immediately be said that we do not propose here a general method of recording complex amplitude without interference. Our system cannot sense any phase modulations that happen between the object and the recording system. However, let us look at a 3-D object illuminated by a coherent plane wave. If the reflected beam from the object propagates in free space and then through the particular optical system, the result at the output plane is some complex amplitude. We claim that this complex amplitude can be restored under incoherent conditions. Once this complex function is in computer memory, we can encode it to a CGH. When this CGH is illuminated by a plane wave, which then propagates through the same optical system mentioned above, the image of the 3-D object is reconstructed in space as a common holographic image. We record several digital pictures of the object from different points of view. The pictures are recorded into a digital computer, which computes a CGH from the input data. Illuminating this hologram by a plane wave reconstructs the original objects and creates the volume effect in the observer's eyes. The hologram that we would like to produce is of the type of a Fourier hologram. This means that the image is reconstructed in the vicinity of the back focal plane of a spherical lens when the hologram is displayed on the front focal plane.

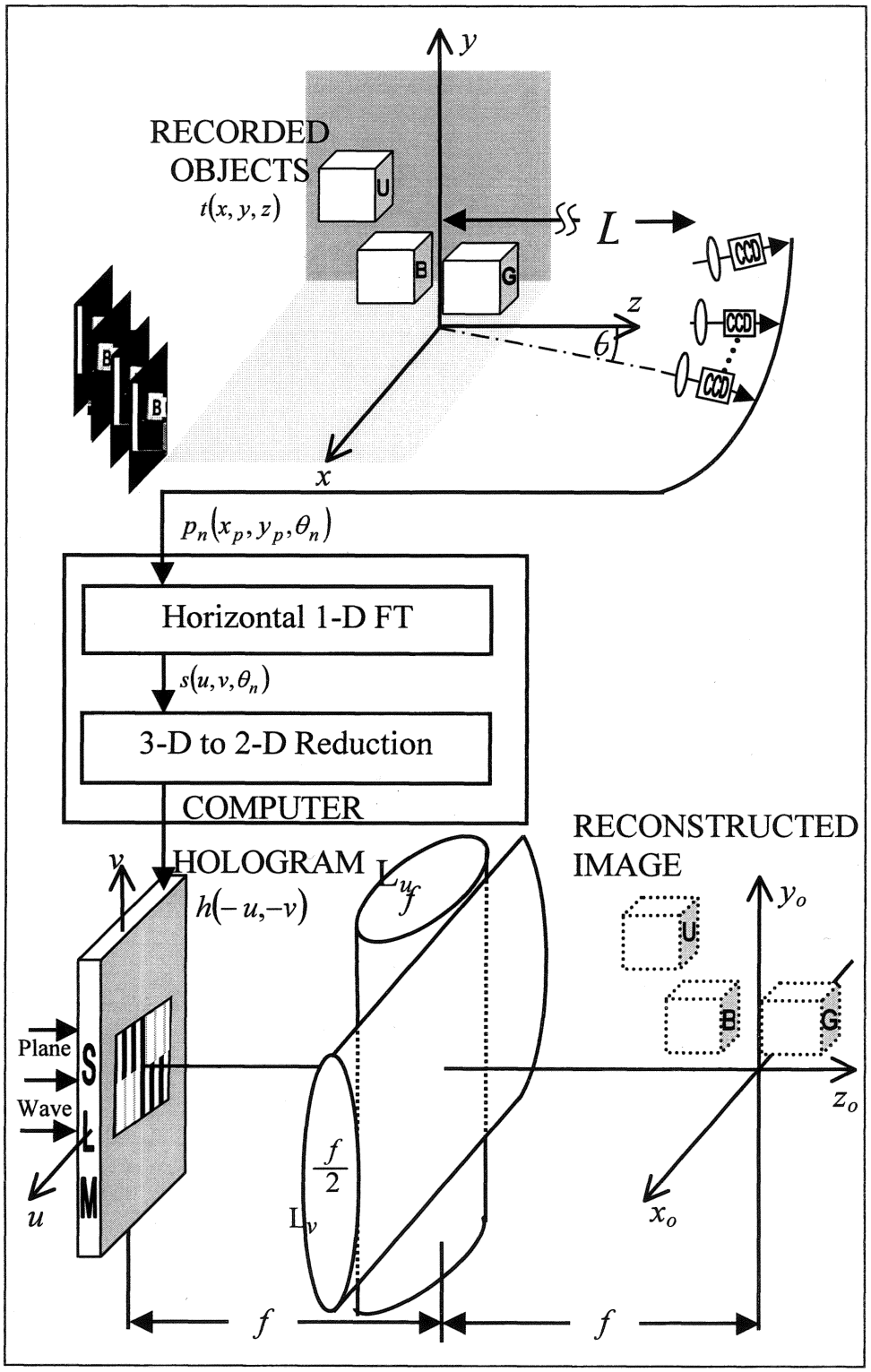

Fig. 1. Schematic of the holographic recording and reconstructing systems.

However, a complete 2-D Fourier hologram can be recorded if the camera's points of view are on a 2-D transverse grid of points. Because it is technically impractical, or at least quite difficult, to shift the camera out of the horizontal plane along a 2-D transverse grid of points, the hologram that we produce in this stage is only a one-dimensional (1-D) Fourier hologram along the horizontal axis and an image hologram along the vertical axis. Consequently, the coherent system that we emulate and the reconstructing system are both composed of a cylindrical Fourier lens in the horizontal axis and a second cylindrical imaging lens in the vertical axis. Next we describe the recording process in detail.

2.1. RECORDING AND SYNTHESIZING THE COMPUTER–GENERATED HOLOGRAM

The recording setup is shown in the upper part of Fig. 1. A 3-D object function $t(x,y,z)$ is located at the coordinate system (x,y,z). $t(x,y,z)$ represents the intensity reflected from all the observed bodies in the scene. From each point of view, the camera observes the scene through an imaging lens located at a distance L from the origin of (x,y,z). The camera is actually shifted in constant angular steps along a horizontal arc centered about the origin, and it is always directed to the origin. The angle between the camera's optical axis and the z axis is denoted θ_n. For each θ_n, the projected image $p_n(x_p,y_p,\theta_n)$ is recorded into the computer, where (x_p,y_p) are the coordinates of the image plane of each camera. On the basis of simple geometrical considerations, the relation between (x_p,y_p,θ_n) and (x,y,z) is given by

$$(x_p, y_p) = (x\cos\theta_n + z\sin\theta_n, y). \tag{1}$$

For simplicity, we assume that the magnification factor of the imaging lens is 1. Also, because distance L is much greater than the depth of the object, all the object points are equally imaged with the same magnification factor of 1. Inside the computer, each projected function is Fourier transformed along horizontal axis x_p only and is imaged along vertical axis y_p. We assume that the digital 1-D Fourier transform (FT) is a perfect imitation of an optical system with the same scaling factor, such that the collection of 1-DFTs is given by

$$s(u,v,\theta_n) \propto \iint p_n(x_p, y_p, \theta_n)\exp(-i2\pi u x_p/\lambda f)\delta(v - y_p)dx_p dy_p, \tag{2}$$

where δ is the Dirac delta function, λ is the wavelength of the plane wave illuminating the system and f is the focal length of the cylindrical Fourier lens.

Let us consider now the relation between $p_n(x_p,y_p,\theta_n)$ and the object $t(x,y,z)$. For a single infinitesimal element of size $(\Delta x,\Delta y,\Delta z)$, at point (x',y',z'), with the intensity $t(x',y',z')$ from the entire 3-D object function, the distribution on the (u,v) plane for each θ_n value is

$$s'(u,v,\theta_n) \propto t(x',y',z')\exp(-i2\pi u x_p/\lambda f)\delta(v - y_p)\Delta x\Delta y\Delta z. \tag{3}$$

Relation (3) is obtained from relation (2) because, for each θ_n value, a single point at the input scene is imaged to a point at the (x_p,y_p) plane. The δ function in relation (3) is a mathematical idealization of the fact that the point at y_p is imaged to the line $v=y_p$ on the (u,v) plane. Substituting Eq. (1) into relation (3) yields

$$s(u,v,\theta_n) \propto t(x',y',z')\exp[-i2\pi(ux'\cos\theta_n + uz'\sin\theta_n)/\lambda f]\delta(v - y')\Delta x\Delta y\Delta z. \tag{4}$$

Next we examine the influence of all points of the object $t(x,y,z)$ on the distribution of $s(u,v,\theta_n)$. The object is 3-D, and the FT operates only along the horizontal axis, whereas along the vertical axis the picture is perfectly imaged. Therefore the overall distribution of $s(u,v,\theta_n)$ is obtained by a 3-D integral of the expression in relation (4) as follows:

$$s(u,v,\theta_n) \propto \iiint t(x,y,z)\exp[-i2\pi(ux\cos\theta_n + uz\sin\theta_n)/\lambda f]\delta(v - y)dxdydz\ . \tag{5}$$

Relation (5) describes a tomographic process in the visible-light regime. By an appropriate Fourier transform from the spatial frequency coordinates[26] $(f_x,f_z)=(u\cos\theta_n,u\sin\theta_n)$ to (x,z), the 3-D object $t(x,y,z)$ can be digitally reconstructed from $s(u,v,\theta_n)$ inside the computer. However, it is not our intention here to deal with tomography or with digital reconstruction. Our goal is to pull out from the entire 3-D distribution given in relation (5) a particular 2-D distribution only. This 2-D distribution, when it is encoded into a CGH and illuminated properly, yields a holographic reconstruction of the object. The maximum range of angle θ_n is chosen to be small (no more than 16° on each side in the present example). Therefore we are allowed to use the following small-angle approximations: $\cos\theta_n\approx 1$ and $\sin\theta_n\approx\theta_n$. Recalling our original goal to get a 2-D hologram containing the information on the objects' volume, we next reduce the 3-D function given by relation (5) to a 2-D function. From the 3-D function $s(u,v,\theta_n)$, we take only the 2-D data that exist on the mathematical plane defined by the equation $\theta_n=au$ in the (u,v,θ_n) space, where a is some chosen parameter. Substituting this condition with the small angle approximations into relation (5) yields the following 2-D function:

$$h(u,v) = s(u,v,\theta_n = au)\Big|_{\substack{\cos\theta_n = 1 \\ \sin\theta_n = \theta_n = au}}$$
$$= \iiint t(x,y,z)\delta(v-y)\exp\left[-i2\pi\left(ux + au^2 z\right)/\lambda f\right]dxdydz\,. \qquad (6)$$

Let us summarize the process up to this point: The 3-D object $t(x,y,z)$ is recorded from several angle values θ_n. In the computer the recorded data of projections of the scene are designated $p_n(x_p,y_p,\theta_n)$. For each value of θ_n, each matrix is Fourier transformed along x_p and imaged along y_p. The 3-D matrix obtained is designated $s(u,v,\theta_n)$. Finally, from the entire 3-D matrix we select only the 2-D matrix with all the values that satisfy the equation $\theta_n = au$.

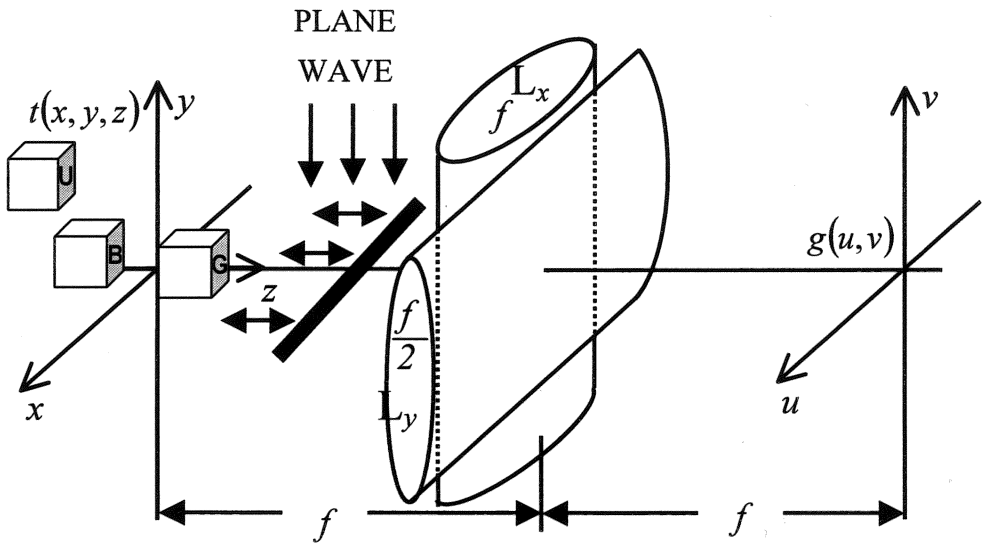

Fig. 2. Equivalent optical systems for the hologram recording.

Next we show that, if a is chosen to be a=-1/(2f), $h(u,v)$ is equal to the complex amplitude on the output plane of the equivalent coherent system, shown in Fig. 2. It should be emphasized that this coherent system is only the equivalent optical system for the expression in relation (6), and we depict it in Fig. 2 only to clarify the equivalent model. The complex amplitude is examined at the back focal plane of a convex cylindrical lens (horizontally focusing) when a plane wave s reflected from the 3-D object $t(x,y,z)$ located at the back focal plane and is perfectly imaged along the vertical axis. For a single infinitesimal element of the size $(\Delta x,\Delta y,\Delta z)$ from the entire object with an amplitude of $t(x',y',z')$, the complex amplitude at the plane (u, v) is[27]

$$g'(u,v) = At(x',y',z')\delta(v-y)\exp\left[\frac{-i2\pi}{\lambda}\left(\frac{ux}{f} - \frac{u^2 z}{2f^2}\right)\right]\Delta x\Delta y\Delta z, \qquad (7)$$

where A is a constant. Summation over the contributions from all the points of the 3-D object yields the following complex amplitude:

$$g(u,v) = A\iiint t(x,y,z)\delta(v-y)\exp\left[\frac{-i2\pi}{\lambda}\left(\frac{ux}{f} - \frac{u^2 z}{2f^2}\right)\right]dxdydz\,. \qquad (8)$$

Comparing Eqs. (8) and (6), we see indeed that substituting a=-1/(2f) into Eq. (6) yields an expression similar to the one given in Eq. (8). The only difference is that $t(x,y,z)$ in Eq. (8) represents a complex amplitude, whereas in Eq. (6) it represents an intensity. As the intensity of the reconstructed object from $h(u,v)$ is proportional to $|t(x,y,z)|^2$, its graytone distribution is expected to be deformed compared with the gray-tone map of the original object. However, we can compensate for this deformation by computing the square root of the grabbed pictures in the recording stage. In both functions $h(u,v)$ and $g(u,v)$ the object's 3-D structure is preserved in a holographic manner. This means that the light

diffracted from the hologram is focused into various transverse planes along the propagation axis according to the object's 3-D structure. Parameter a can in fact take any arbitrary real value, not just the value $-1/(2f)$. In that case, after integration variable z is changed to $z'=-2faz$, Eq. (6) becomes

$$h(u,v) \propto \iiint t\left(x, y, \frac{-z'}{2af}\right)\delta(v-y)\exp\left[\frac{-i2\pi}{\lambda}\left(\frac{ux}{f}-\frac{u^2 z'}{2f^2}\right)\right]dxdydz'. \qquad (9)$$

Relation (9) also has the form of Eq. (8) but with the change that the hologram obtained describes the same object on a different scale along its longitudinal dimension z. We conclude that by our choice of parameter a we can control the longitudinal magnification of the reconstructed image, as we show below.

Equation (8) represents a complex wave front, which usually should be interfered with a reference wave to be recorded. In the case of wave interference the intensity of the resultant interference pattern keeps the original complex wave front in one of four separable terms. However, in our case the complex wave-front distribution is recorded into computer memory in the form of Eq. (6) [or relation (9)] without any interference experiment and actually without the need to illuminate the object with coherent laser light. Because the expression in Eq. (6) describes the equivalent of a wave-front distribution, it contains 3-D holographic information on the original objects, which can be retrieved as described in what follows.

As we mentioned above, the hologram values are stored in computer memory in the form of the complex function $h(u,v)$. To reconstruct the image from the hologram, the computer should modulate some transparency medium with the hologram values. If the transparency cannot be modulated directly with complex values, one of many well-known coding methods for CGHs[28] might be used. The spatial light modulator (SLM) that we use in this study can modulate the intensity of light with continuous gray tones. Therefore, complex function $h(u,v)$ is coded into a positive real transparency as follows,

$$h_r(u,v) = 0.5\left(1 + \mathrm{Re}\left\{h(u,v)\exp\left[\frac{i2\pi}{\lambda f}\left(d_x u + d_y v\right)\right]\right\}\right), \qquad (10)$$

where (d_x,d_y) is the new origin point of the reconstruction space and $|h(u,v)|$ is normalized at 0–1. The holographic reconstruction setup is shown in the lower part of Fig. 1. To get the output image with the same orientation as the object, we display the 180°-rotated hologram $h(-u,-v)$ on the SLM. Then the SLM is illuminated by a plane wave, which propagates through the SLM and the two cylindrical lenses with two orthogonal axes. Through lens L_u, a 1-D FT of $h(-u,-v)$ along u is obtained at the back focal plane along x_o. Lens L_v images the distribution along the v axis on the y_o axis. This optical setup is identical to the equivalent coherent system shown in Fig. 2, and therefore the real image of the original 3-D object is reconstructed in the vicinity of the back focal plane of cylindrical lens L_u.

To calculate the magnification of the image along each axis we consider the equivalent optical process on object and on image planes. Based on Eq. (6) together with the operation of lens L_u, the effective system from plane (x,y) to the output plane, along the horizontal axis, is similar to a 4-f system. Therefore the overall horizontal magnification is identical to 1. In the vertical axis the object is imaged twice from plane (x,y) to output plane (x_o,y_o), and therefore the magnification is also equal to 1. On the longitudinal axis the situation is a bit more complicated. Looking at Eq. (6) and the Fourier lens L_u, we see a telescopic system but with two different lenses. From Eq. (6) the effective focal length of the first lens is $f_1 = \sqrt{f/(2|a|)}$. The focal length of reconstructing lens L_u is $f_2=f$. Using the well-known result that the longitudinal magnification of a telescopic system is $(f_2/f_1)^2$, we find the longitudinal magnification in our case to be $2f|a|$. Note that with parameter a one can control the image's longitudinal magnification independently of the transverse magnification.

2.2. Experimental results

In our experiment the recording was carried out by the system shown in the upper part of Fig. 1 and the reconstruction was demonstrated first by a computer simulation of the system shown in the lower part of Fig. 1 and then by an optical experiment. The scene observed contains three cubes of size 5cm×5cm×5cm located at different distances from the camera.

We show in Fig. 3 16 examples selected from 65 scene viewpoints taken by the camera. Each projection contains 256×256 pixels, and observed by the CCD from a distance of 77 cm. The angular range is ±16° from the CCD axis to the z axis, and the angular increment between every two successive projections is 0.5°.

The hologram was computed from the set of the 65 projections according to the procedure described above. Explicitly, for each picture, every row in every projection matrix was Fourier transformed. From the entire 3-D matrix obtained, we picked only the 2-D matrix placed on the diagonal plane expressed by the equation $\theta_n=au$. The magnitude and the phase angle of the computed 256×256-pixel complex function $h(u,v)$ are shown in Figs. 4(a) and 4(b), respectively. The central

part of the CGH computed according to Eq. (10) is depicted in Fig. 4(c). The total size of the CGH is 800 pixels on the horizontal axis and 256 pixels on the vertical axis.

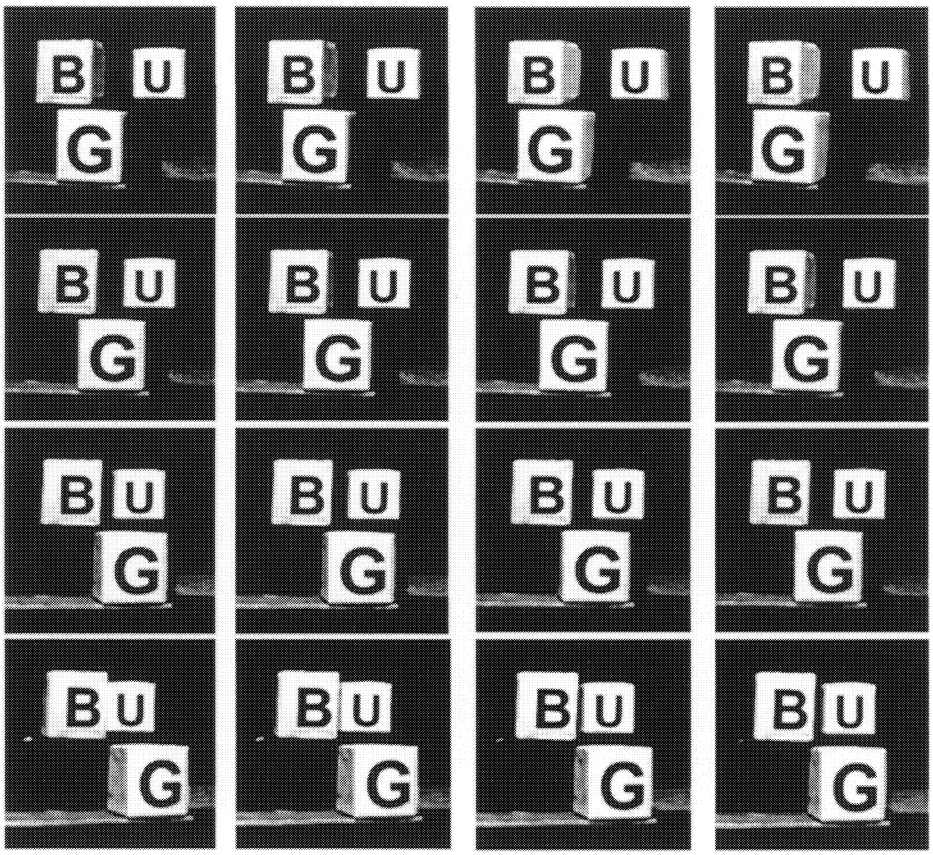

Fig. 3. Sixteen projections of the sixty-five projections of the input scene taken by the camera from various viewpoints.

The reconstruction results from the hologram obtained from the computer simulation are depicted in Fig. 5. We obtained these results by calculating the diffraction behind the cylindrical lenses[29] for three values of z_o. Figure 5 shows the reconstructed intensity at three transverse planes along the optical axis. The figure shows the central three horizontal diffraction orders, whereas the zero order appears as the white area in the center of each part of Fig. 5; this area is thinner in Fig. 5(b) than in Figs. 5(a) and 5(c). At each transverse plane, in the left-hand diffraction order a different letter of a different cube is in focus; thus reconstruction of the 3-D objects is demonstrated.

In the optical experiment the CGH [part of which is shown in Fig. 4(c)] was displayed on a SLM. Parameter a in this example was chosen to be $[\sin(32°)/3.5]\text{cm}^{-1}$, where 32° is the angular range of the capturing camera and 3.5 cm is the width of the SLM located in the (u,v) plane. The reconstruction results in the region of the left-hand diffraction order are shown in Fig. 6 at three transverse planes along the optical axis. Evidently, the same effect in which every letter is in focus on a different transverse plane appears also in Fig. 6.

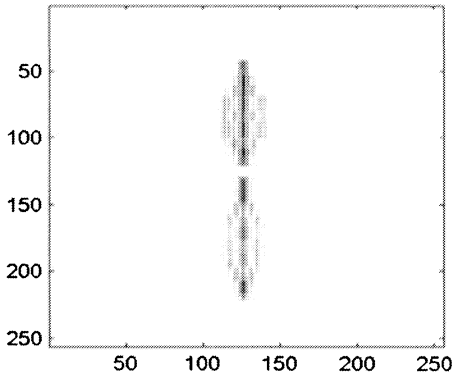

(a)

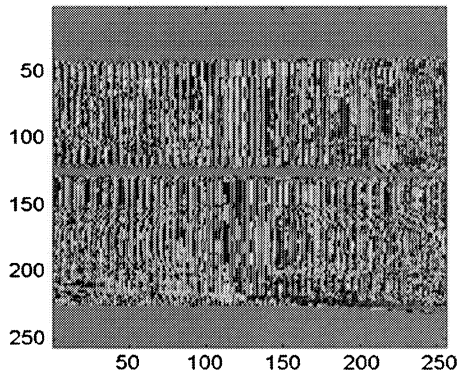

(b)

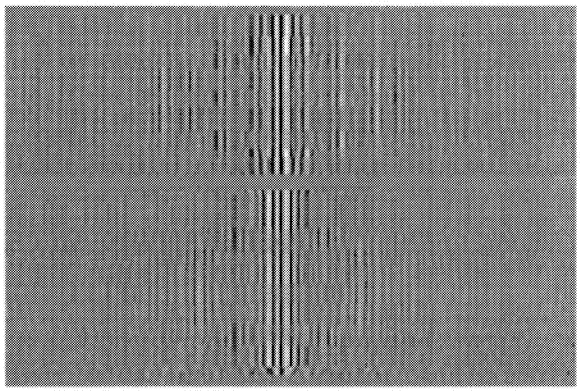

(c)

Fig. 4. (a) Magnitude (the maximum value is darkest) and (b) phase angle (π is white and 2π is black) of the hologram recorded and computed in the experiment. (c) Central part of the CGH, computed by Eq. (10) from the complex function shown in (a) and (b).

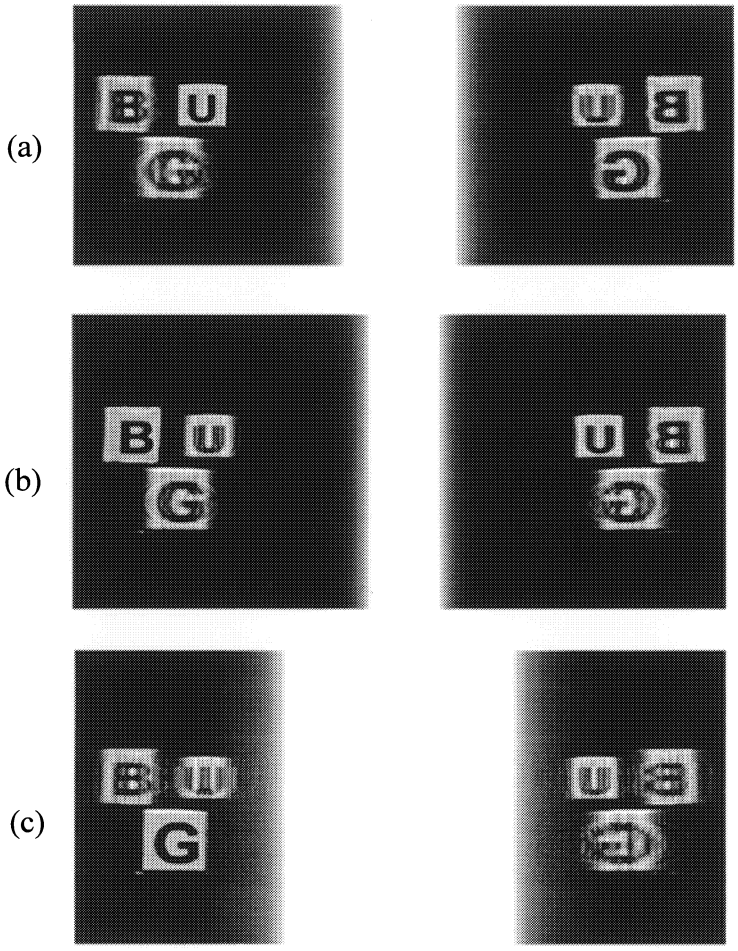

Fig. 5. Simulation results from the hologram shown in Fig. 4(c) at the vicinity of the back focal point of lens *Lu* for three transverse planes at (a) z_o=-9*f*, (b) z_o=6*f*, (c) z_o= 25*f*.

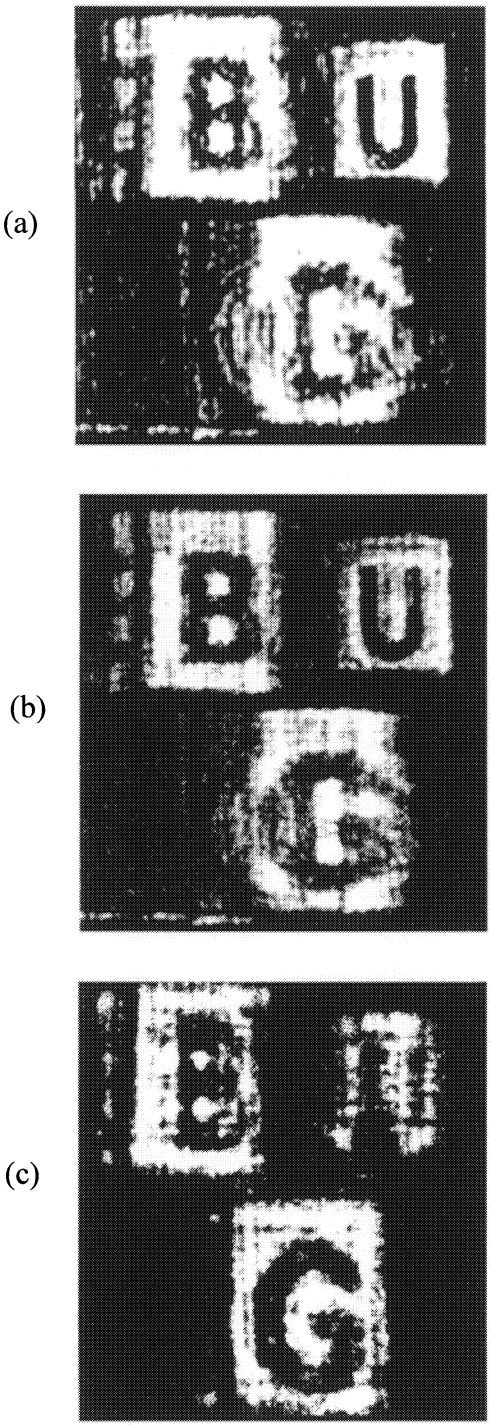

Fig. 6. Experimental results from the hologram shown in Fig. 4(c) at the vicinity of the back focal point of L_u for three transverse planes at (a) z_o= -0.5 cm, (b) z_o=2.5 cm, (c) z_o=6 cm.

3. TWO-DIMENSIONAL FOURIER HOLOGRAM OF 3-D SCENE

In the present section we suggest a new procedure for generating a CGH of general 3-D objects. This procedure creates the CGH by fusing the angular projections of computer-designed 3-D objects. The same algorithm can be employed on a set of angular perspectives of realistic objects captured by a digital camera from some realistic scene, as actually demonstrated in section 2. However, the present algorithm is different from that of section 2, where the scene was observed only from horizontal viewpoints. Here we move the viewpoint in both horizontal and vertical directions. By performing a particular computation on the entire set of angular perspectives of the 3-D object, a 2-D complex function is obtained. This function is equal to the complex amplitude of a coherent-light wave front, diffracted from the same object, and then propagates through a spherical lens as far as the rear focal plane. This complex function is then encoded by a conventional procedure to a CGH with real and positive transparency values. Illuminating the CGH by a plane wave reconstructs the original object and creates the volumetric effects. It should be emphasized that, once all the projections are available in the computer memory, the computation complexity of the hologram is equivalent to that of a 2-D Fourier transform, and thus the CGH is computed in a relatively short time without sacrificing image quality.

Although the input data in our method are the set of the object's angular viewpoints, it should be emphasize once again that our algorithm differs from other algorithms in general and from the stereoscopic[16,18] and multiplex CGHs in particular. Unlike the stereoscopic hologram, our CGH is a single Fourier hologram in which every hologram point contributes a fraction of the light to the entire constructed 3-D image, and each point of the constructed image is obtained by light diffracted from the entire CGH. All the angular projections are fused together in a particular mathematical procedure to yield a single Fourier hologram that is equivalent to an optical Fourier hologram recorded by a coherently illuminated 2-*f* system[30] (but with a 3-D object as the system's input). However, the complex wave-front distribution on the Fourier plane is calculated in the computer without any interference experiment. Since the resulting hologram is similar to a Fourier hologram, the reconstruction stage will be carried out by a Fourier lens, as described in the following sections.

3.1. Projection-Based Algorithm For Synthesizing A Computer-Generated Hologram

The first step in our algorithm of synthesizing the CGH is to create in the computer memory a 3-D object that later will be reconstructed by this CGH. Next, the set of the object's angular projections are computed. Then a series of mathematical operations are done on the set of projections, the end product of which is a single 2-D complex matrix. Finally, the complex matrix is coded to a real and positive-valued matrix to be used as a holographic transparency.

Let us describe this series of steps more rigorously. The object denoted by $t(x,y,z)$ is defined in a Cartesian coordinate system (x,y,z) as shown in the upper part of Fig. 7, where z is the longitudinal axis (the virtual optical axis). For each pair of angles φ_m,θ_n in the horizontal and vertical directions, respectively, the m, nth perspective of the object is computed. For each φ_m,θ_n, the projected image $P_{mn}(x_p,y_p)$ is recorded in the computer memory as a 2-D matrix, where (x_p,y_p) is the coordinate system of each projection. With use of well-known geometrical considerations, the relation between (x_p,y_p) and (x,y,z) is given by[31]

$$\begin{aligned} x_p &= x\cos\varphi_m - z\sin\varphi_m, \\ y_p &= y\cos\theta_n - z\sin\theta_n\cos\varphi_m - x\sin\varphi_m\sin\theta_n. \end{aligned} \tag{11}$$

In the next step of the algorithm, each projected image from the view angle (φ_m,θ_n) is multiplied by the exponential function $\exp[-i2\pi b(x_p\sin\varphi_m+y_p\sin\theta_n)]$. This product is then summed to get a single complex value in the following way:

$$s(m,n) \propto \iint p_{mn}(x_p,y_p)\exp\left[-i2\pi b\left(x_p\sin\varphi_m + y_p\sin\theta_n\right)\right]dx_p\,dy_p, \tag{12}$$

where b is a real-valued constant. The next projected image, viewed from an adjacent point having a small incrementally changed angle, is calculated, and a new value, say $s(m+1,n)$, is obtained. The values obtained from Eq. (12) are assembled into a complex matrix. Every value of this matrix corresponds to a different point of view and the matrix is arranged in the same order as the projected images are observed. However, as we show later, the connections between the hologram points and the various perspectives exist only in the synthesis stage. In the image reconstruction stage, the resulting hologram is global in the sense that each point of the hologram is radiated onto the entire volumetric image. Since the matrix values are complex, the hologram must be coded into real and nonnegative values of a holographic

transmittance, as described in Section 3.3. When this coded matrix is coherently illuminated, it yields a holographic reconstruction of the object. The complete computational process is illustrated schematically in the center of Fig. 7; the reconstruction stage is shown in the lower part of the figure. The mathematical verification of this algorithm is described in detail in Section 3.2.

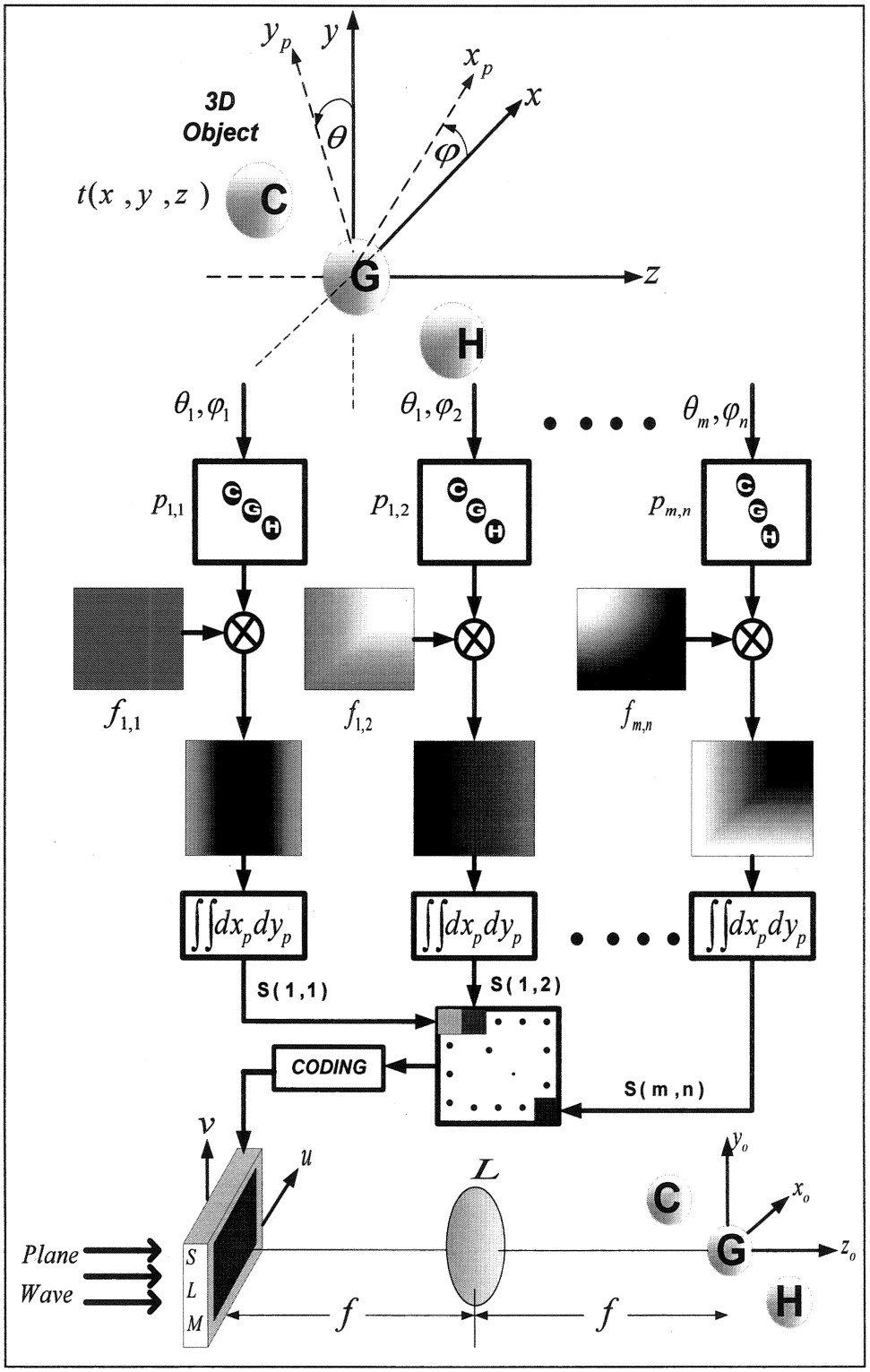

Fig. 7. Schematic of the computational process of the CGH and of the image construction from the CGH. $f_{m,n}=\exp[-i2\pi b(x_p\sin\varphi_m+y_p\sin\theta_n)]$.

3.2. Equivalence between the algorithm and recording a Fourier hologram

In this section we show that the proposed CGH algorithm is an imitation of a particular holographic coherent system. Therefore, the constructed image has features similar to those of an image reconstructed from a coherently recorded hologram. The analogy between the optical system and the computation procedure has already been described in detail in section 2 for horizontal projections only. Here the situation is different, and therefore, we analyze the case of bidirectional projections in detail.

Let us look at a single infinitesimal element of size $(\Delta x,\Delta y,\Delta z)$ from the entire 3-D object shown in Fig. 7. This element at the point (x,y,z) with value $t(x,y,z)$ appears as a single element on every projection plane (x_p,y_p), but at a different location from one projection to another. Based on Eq. (12), the distribution on the hologram plane for all (φ_m,θ_n) values, and for a single source point, is

$$\begin{aligned} s'(m,n) &= \iiint t(x,y,z)(\Delta x\Delta y\Delta z)\delta(\bar{x}_p - x_p, \bar{y}_p - y_p) \\ &\quad \times \exp\left[-i2\pi b\left(\bar{x}_p \sin\varphi_m + \bar{y}_p \sin\theta_n\right)\right] d\bar{x}_p d\bar{y}_p \\ &= t(x,y,z)\exp\left[-i2\pi b\left(x_p \sin\varphi_m + y_p \sin\theta_n\right)\right](\Delta x\Delta y\Delta z). \end{aligned} \tag{13}$$

Substituting Eq. (11) into Eq. (13) yields

$$\begin{aligned} s'(m,n) = t(x,y,z)\exp\{-i2\pi b[&\sin\varphi_m(x\cos\varphi_m - z\sin\varphi_m) \\ &+ \sin\theta_n(y\cos\theta_n - z\sin\theta_n\cos\varphi_m - x\sin\varphi_m\sin\theta_n)]\}(\Delta x\Delta y\Delta z). \end{aligned} \tag{14}$$

Since the input virtual scene is 3-D, the overall distribution of $s(m,n)$ resulting from the points of the entire scene is obtained as a volume integral of all the points from the input scene, as follows:

$$\begin{aligned} s(m,n) &= \iiint s'(m,n)dxdydz \\ &= \iiint t(x,y,z)\exp\{-i2\pi b[\sin\varphi_m(x\cos\varphi_m - z\sin\varphi_m) \\ &\quad + \sin\theta_n(y\cos\theta_n - z\sin\theta_n\cos\varphi_m - x\sin\varphi_m\sin\theta_n)]\}dxdydz\,. \end{aligned} \tag{15}$$

The maximum view angles $(\varphi_{max},\theta_{max})$ are chosen to be small, and thus the small-angle approximations $\cos\varphi_m\approx 1$ and $\cos\theta_n\approx 1$ can be applied. Substituting this approximation in Eq. (15) yields

$$\begin{aligned} s(m,n) \cong \iiint t(x,y,z)\exp\{&-i2\pi b[x\sin\varphi_m + y\sin\theta_n \\ &- z(\sin^2\varphi_m + \sin^2\theta_n) - x\sin^2\theta_n\sin\varphi_m]\}dxdydz\,. \end{aligned} \tag{16}$$

Under conditions of small view angles, the term $x_s\sin^2\theta_n\sin\varphi_m$ in the exponent of Eq. (16) is much smaller than one radian for the whole range of the variables. Therefore, this term can be neglected. When the matrix $s(m,n)$ is displayed on any optical transparency, and assuming the angular increment from one projection to another is infinitesimally small, one can change variables of the function s from (m,n) to continuous variables (u,v) as in the following:

$$\begin{aligned} s(m,n) \cong \iiint t(x,y,z)\exp\Bigg\{&\frac{-i4\pi b\sin\varphi_{max}}{\Delta u} \\ &\times\left[xu + yv - z\frac{2\sin\varphi_{max}}{\Delta u}\left(u^2+v^2\right)\right]\Bigg\}dxdydz\,. \end{aligned} \tag{17}$$

In deriving Eq. (17) from Eq. (16), we assume that there is an equal angular interval between any two successive projections. In other words, we use the relation $\sin\varphi_m = m\sin\varphi_{max}/M$ and $\sin\theta_n = n\sin\theta_{max}/N$, where M and N are the total number of projections in the horizontal and vertical directions, respectively. It is also assumed in Eq. (17) that the hologram can be displayed on the SLM such that the equality $\sin\varphi_{max}/\Delta u = \sin\theta_{max}/\Delta v$ is satisfied, where Δu and Δv are the width and the height of the transparency medium, respectively.

It is now shown that $s(u,v)$ of Eq. (17) has the same functional behavior as the complex amplitude on the output plane of the equivalent coherent system. This coherently illuminated setup is the equivalent optical system for the digital process that yields the hologram described in Eq. (17). The 3-D object $t(x,y,z)$ is illuminated by a plane wave of wavelength λ, and the reflected wave front from the object propagates through a spherical lens with focal length f. The complex amplitude obtained at the back focal plane is given by[24]

$$g(u,v) = c\iiint t(x,y,z)\exp\left[-i\frac{2\pi}{\lambda f}\left(xu + yv - z\frac{u^2+v^2}{2f}\right)\right]dxdydz\,, \tag{18}$$

where C is a constant and $g(u,v)$ represents a complex wave front, which should be interfered with a reference wave in order to be recorded as a Fourier hologram. In the case of wave interference, the intensity of the resulting interference pattern keeps the original complex wave front in one of four separable terms.[30] The expressions in Eq. (17) and Eq. (18) are functionally equivalent and the differences exist only in the constants of the exponent power. Therefore, $s(u,v)$ is a 2-D function which contains 3-D information of the object similar to the way that a 2-D optical hologram contains the 3-D information of a recorded object. In both functions $s(u,v)$ and $g(u,v)$, the object's 3-D structure is preserved in a holographic manner. This means that light diffracted from the hologram is focused into different transverse planes along the propagation axis according to the object's 3-D structure.

This is the right place to re-emphasize that we do not synthesize here a multiplex CGH. As proved above, the entire reconstructed volumetric image gets light from each point of $s(u,v)$ and the entire distribution of $s(u,v)$ contributes energy to each point on the volume of the reconstructed object. The situation here is definitely dissimilar to the multiplex hologram in which different subholograms generate different 2-D images for different viewer perspectives to create all together the effect of a 3-D object. The origin of this common confusion, which relates our algorithm to the multiplex hologram, is the similarity in the nature of the input data. The two methods start their computation process from similar input data of multiple perspectives of the object. However, at this point the similarity between the two holograms begins and ends. This is because in our algorithm all of the input perspectives are fused together into a final hologram in which no part can be related to any particular image perspective or any other part of the reconstructed image.

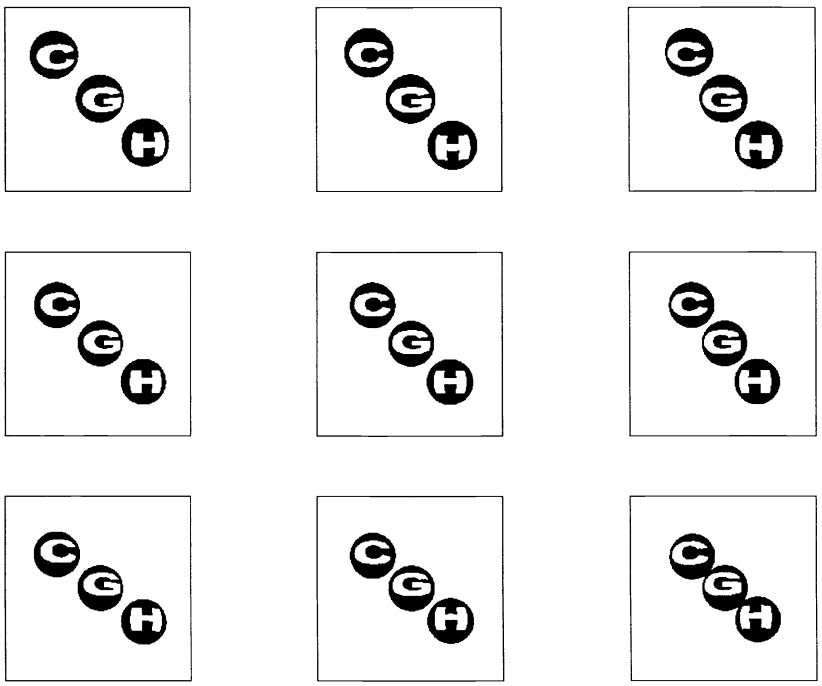

Fig. 8. Nine projections of the 3-D objects projected from various viewpoints.

Assuming that the object is constructed by a lens with focal length f and by a plane wave of wavelength λ, the magnifications of the image along the three axes are

$$M_x \equiv \frac{\bar{x}_s}{\bar{x}_o} = \frac{2\lambda f b \sin\varphi_{\max}}{\Delta u}, \; M_y \equiv \frac{\bar{y}_s}{\bar{y}_o} = \frac{2\lambda f b \sin\theta_{\max}}{\Delta v} = M_x,$$

$$M_z \equiv \frac{\bar{z}_s}{\bar{z}_o} = 8\lambda b\left(f\frac{\sin\varphi_{\max}}{\Delta u}\right)^2, \tag{19}$$

where $(\bar{x}_s, \bar{y}_s, \bar{z}_s)$ and $(\bar{x}_o, \bar{y}_o, \bar{z}_o)$ are the sizes of the object in the input space and in the output space, respectively. The ratio between the longitudinal magnification to each transversal magnification is

$$\frac{M_z}{M_x} = \frac{4f\sin\varphi_{\max}}{\Delta u} = \frac{M_z}{M_y}. \tag{20}$$

These ratios indicate how much the reconstructed image has been shrunk or stretched along the longitudinal axis in relation to its transverse magnifications.

Equation (17) also gives indications of the desired parameters of the algorithm manifested by Eq. (12). One such parameter is the maximum view angles, which are determined by the spatial bandwidth ($2B_x$,$2B_y$,$2B_z$) of the object, according to the following inequalities:

$$b\sin\varphi_{\max} \geq B_x, \;\; b\sin\theta_{\max} \geq B_y, \;\; b\left(\sin^2\varphi_{\max} + \sin^2\theta_{\max}\right) \geq B_z, \tag{21}$$

where the B_i are in units of (pixel)$^{-1}$. The spatial bandwidth is calculated as the number of cycles of the highest meaningful harmonic component in the object's composition divided by matrix size. If inequalities (21) are not satisfied, it is expected that high frequencies will be cut off. From these relations it is clear that the parameter b can guarantee that relations (21) are fulfilled for any given bandwidth without increasing the view angle beyond the small-angle limit. Other parameters that should be determined are the angle increments ($\Delta\varphi$,$\Delta\theta$) between successive projections. Each projection yields a single sample in the Fourier domain, and sampling in the Fourier domain produces replications in the image domain. The angular interval should assure that these constructed replicas do not overlap. Elementary Fourier analysis shows that this sampling condition is fulfilled if

$$(\Delta\varphi, \Delta\theta) \cong (\Delta\sin\varphi, \Delta\sin\theta) \leq \left(\frac{1}{bW_x}, \frac{1}{bW_y}\right), \tag{22}$$

where (W_x,W_y,W_z) are the sizes of the input object in pixels and ($\Delta\varphi$,$\Delta\theta$) are in radians.

3.3. Simulated and optical construction of three-dimensional objects

The proposed algorithm was applied on an example of computer-designed 3-D objects. The construction stage was demonstrated first by a computer simulation of the system shown in Fig. 7, and then by an optical experiment. The purpose of the computer simulation is to demonstrate the potential quality of the image construction from our method in view of the low quality of the SLM as a holographic transparency. The object used for 3-D imaging was composed of three spheres of radius 110 pixels carrying the letters C, G, and H, each of which was located at different depth from the viewer: The C ball was at the back of the scene at point (x,y,z)=(-170,170,-170) pixels, the G ball was at the center of the scene at point (x,y,z)=(0,0,0) and the H ball was at the front of the scene at point (x,y,z)=(170,-170,170) pixels. From each point of view, a projected image of 700×700 pixels was recorded. The angular range was ±10° in all directions with a uniform angular displacement of $\Delta\varphi$,$\Delta\theta$=0.1°. Nine projections (the central and the eight most extreme) of 201×201 scene viewpoints are shown in Fig. 8. The hologram was computed from this set of 201×201 projections of the 3-D scene according to the procedure sketched in Fig. 7. The spectral matrix $s(u,v)$ generated according to Eq. (12) from these data is shown in Fig. 9. The central 100×100 pixels of the magnitude and the phase angle of $s(u,v)$ are shown in Figs. 9(a) and 9(b), respectively. The constructed images from the complex hologram obtained by computer simulation are depicted in Fig. 10. The contrast of all construction results in this study was inverted for a better visualization.

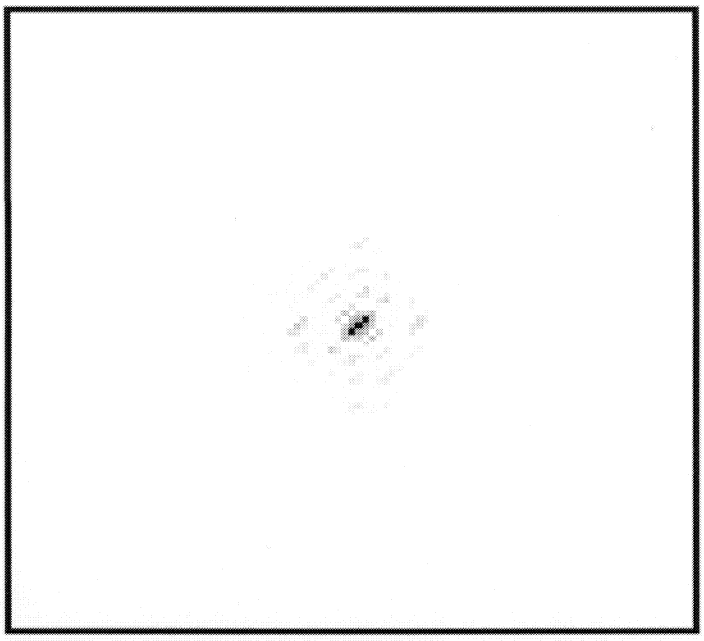

(a)

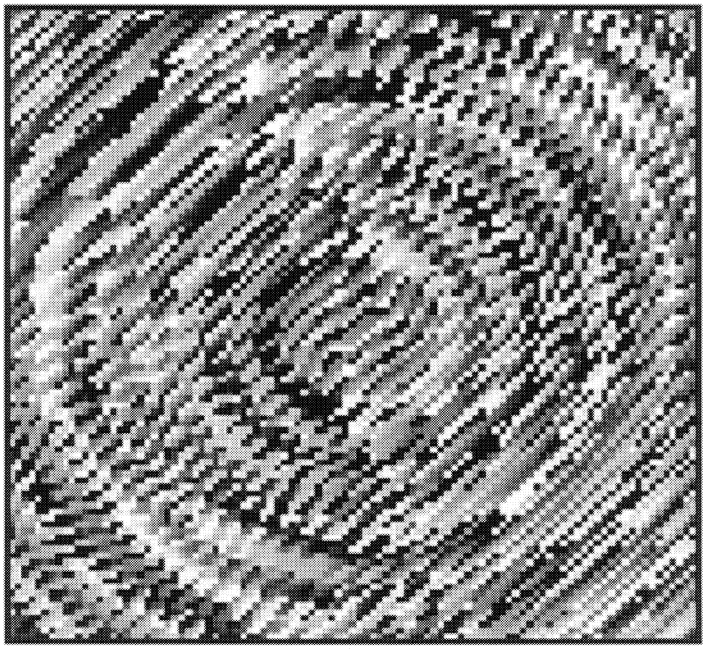

(b)

Fig. 9. Enlarged portion (100×100 pixels of 201×201) of (a) the magnitude and (b) the phase angle of the noncoded CGH generated by the algorithm shown in Fig. 7.

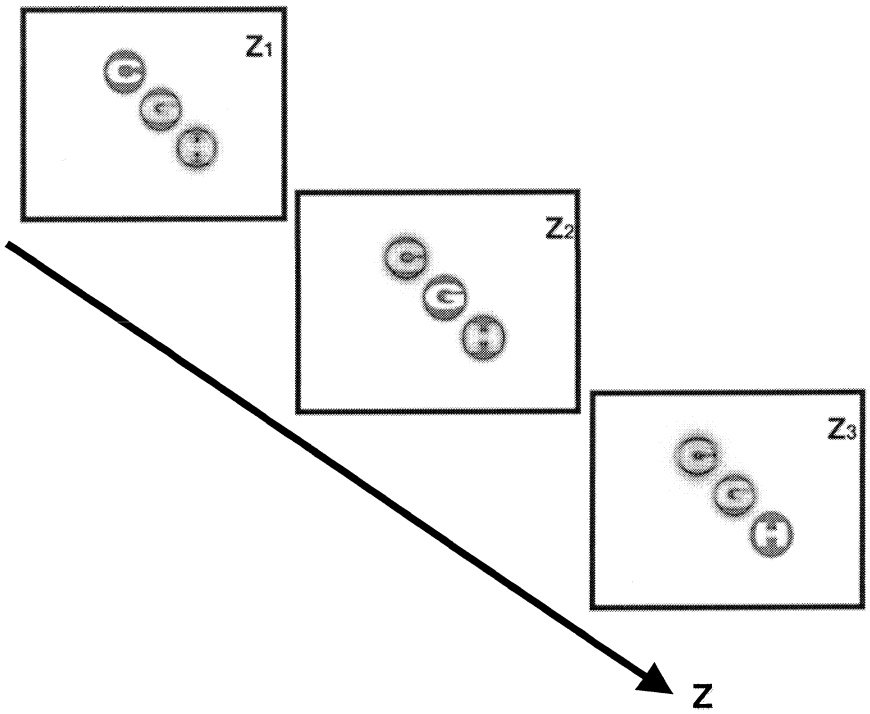

Fig.10. Simulation results from the hologram shown in Fig. 9 at the vicinity of the back focal plane of lens L for three successive transverse

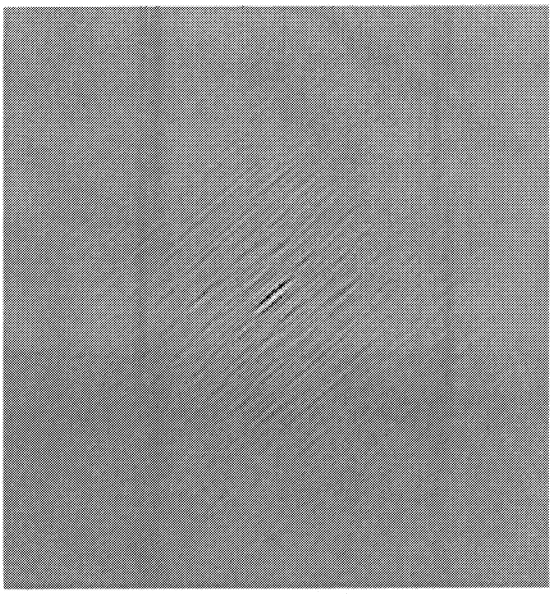

Fig. 11. Central part (300×300 pixels of 640×640) of the CGH computed by Eq. (23) from the complex function shown in Fig. 9.

These results are obtained by calculating the diffraction patterns behind a spherical lens at three different transverse planes along the propagation axis z in the vicinity of the rear focal point. These figures show that at each transverse plane, a different letter of a different ball is in focus; thus construction of the 3-D objects is demonstrated. The optical construction from the CGH is also demonstrated. Since the hologram values are stored in the form of the complex function $s(u,v)$, and the SLM used in this study can modulate the light intensity only with positive gray tones, it is necessary to code $s(u,v)$. The complex function $s(u,v)$ was coded into positive, real transparency $T(u,v)$ according to Burch's method[32]:

$$T(u,v)=\frac{1}{2}\left(1+\mathrm{Re}\left\{s(u,v)\exp\left[i\frac{2\pi}{\lambda f}(d_x u+d_y v)\right]\right\}\right), \tag{23}$$

where (d_x,d_y) is the new origin point of the construction space and $|s(u, v)|$ is normalized between 0 and 1. Note that although Burch's coding method is not efficient, it demands much less computation in comparison with other known iterative coding methodes.[12] Computation is a significant resource which should be considered when one chooses a coding method, especially if the CGH is applied for real-time applications. Moreover, the reconstructed image from such hologram is most similar to the original object. This is because a hologram coded by Burch's method yields in the vicinity of the first diffraction order the exact (neglecting errors caused by a digital sampling and quantization) holographic image of the object. In fact, excluding the zeroth order, Burch's CGH is identical to the conventional optical hologram recorded from the interface between the reference and object beams, and these optical holograms are efficiently useful for many applications. Of course, these comments should not discourage anyone from using or searching for other coding methods that are more efficient in aspects different from those mentioned above, such as diffraction efficiency, space–bandwidth-product, etc.

The central part of 300×300 pixels out of 640×640 pixels of the hologram computed by Eq. (23) is shown in Fig. 11. The coded CGH shown in Fig. 11 was displayed on an SLM. The total size of the hologram on the SLM is $\Delta u\times\Delta v$=17×21 mm. To fulfill the condition $\sin\varphi_{\max}/\Delta u = \sin\theta_{\max}/\Delta v$, only the central 80% of the original hologram along the u axis is displayed on the SLM. This is equivalent to displaying a hologram in which the maximal view angle along the horizontal direction is 8°, while along the vertical direction the maximal view angle is still 10°.

A collimated beam from a He–Ne laser at 632.8 nm illuminates the SLM and propagates through the spherical lens towards the observer. The real image of the computer-designed, 3-D object is constructed in the vicinity of the back focal plane of the lens with a focal length of 750 mm and a diameter of 50 mm. The parameter b in this example was chosen to be equal to 0.9. Figure 12 shows the reconstruction results observed by the CCD for three different transverse planes along the optical axis at distances of 715, 750, and 781 mm (±5 mm) from the lens (the distance between the lens and the SLM was 75 mm). The contrast in these figures has also been inverted for better visualization. Obviously, the same effect, in which every letter is in focus at a different transverse plane, also appears in Fig. 12. In comparison with Fig. 10, the construction of the object is noisier; this is due to the use of the SLM and the speckle nature of the laser. SLMs, although they have not reached the technological level of a good holographic transparency, widen the opportunity of implementing dynamic CGHs. This is the main reason that SLM is preferred here over otherwise more suitable holographic transparencies. The overall diffraction efficiency was measured from simulation of the amplitude hologram and found to be 0.0013% in the coding method given by Eq. (23). This figure is typical of this kind of amplitude hologram and could be increased using a phase-only SLM. The average rms reconstruction error is found to be 0.45%. To verify the validity of Eq. (20), we compared the theoretical against the experimental ratio of the longitudinal to the transverse magnifications. According to Eq. (20), with the parameters f =750 mm, $\varphi_{\max}$=8°, and Δu=17 mm, the ratio between the magnifications is $M_z/M_x=M_z/M_y$=24.6. On the image captured by the CCD at the back focal plane of the lens, the horizontal and vertical gap between two adjacent balls is 153 pixels. For a pixel size of 8.6 μm and 30±5 mm longitudinal gap between every two successive balls, the experimental magnification ratio is between 19 and 26.6. Therefore, the theoretical result is inside the range of the error measurement.

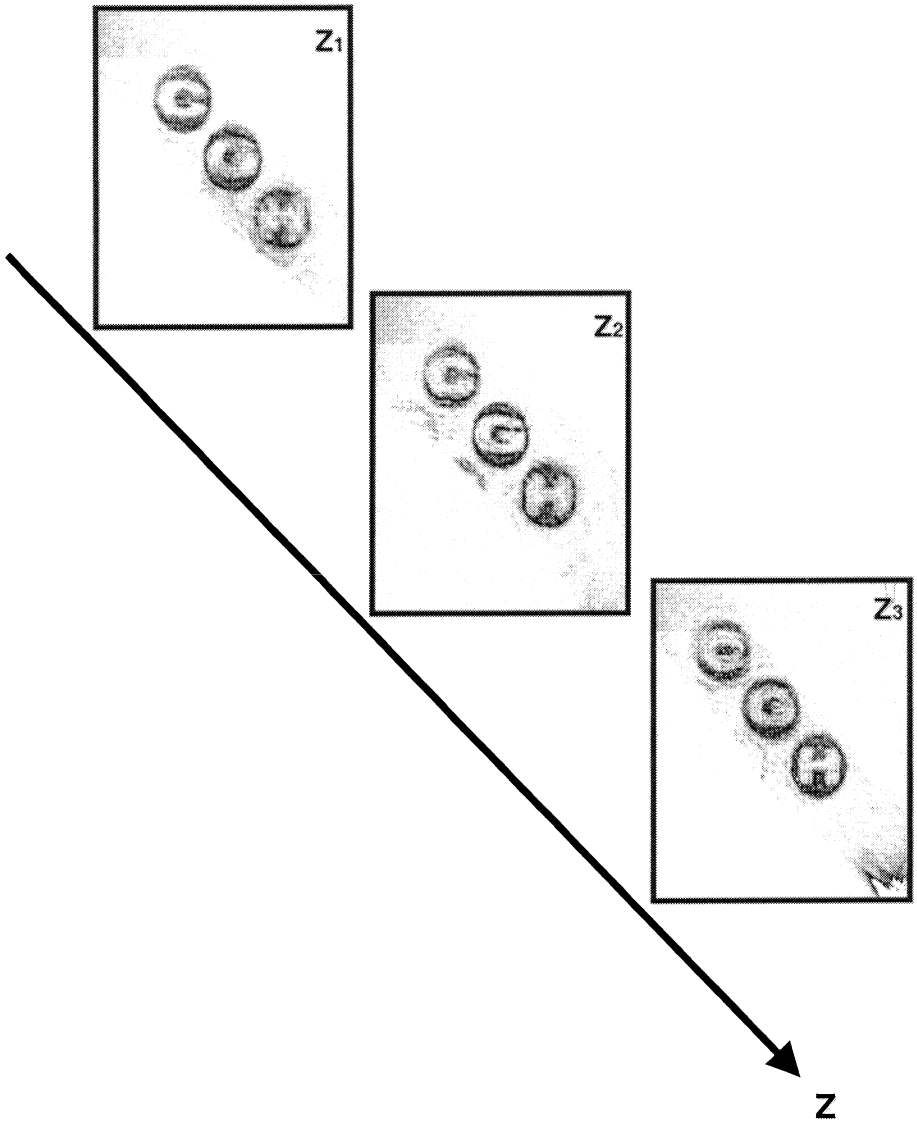

Fig. 12. Experimental results of the first diffraction order obtained from the CGH shown in Fig. 11 at the vicinity of the back focal plane of L for three transverse planes at z_1=715 mm, z_2=750 mm, and z_3=781 mm.

4. CONCLUSIONS

A new process of computing holograms of computer designed 3-D objects has been proposed and demonstrated. By fusion of multiple projections of the object, a 2-D function has been obtained that contains 3-D information of the object. The resulting CGH is equivalent to an optical Fourier hologram of a realistic 3-D scene. The experimental construction was successfully demonstrated, thus indicating the potential of the technique for 3-D displays. Our study shows that the proposed method has the following features. When the set of projections are available in the computer memory, the rest of the computation is equivalent to the computation of 2-D Fourier transforms as manifested by Eq. (12). Therefore, the new method requires less computation time than conventional methods of producing CGHs. This statement should be carefully clarified. Let us assume that the object space contains $N \times N \times N$ pixels. Equation (12) indicates that the number of computational operations is equal to the number of 2-D Fourier transform operations only, i.e., N^2 multiplications and summations. [However, since Eq. (12) is not really a Fourier transform, the fast Fourier transform algorithm cannot be applied here.] The number N^2 is significantly less than the number of operations needed in algorithms that suggest direct superposition[14] of all object points in the 3-D space, which is of the order of N^3 operations. Indeed, this discussion ignores the calculations needed for computing the set of angular projections of the 3-D object. However, note that memorizing a 3-D object in the form of its collection of angular projections is as legitimate as any other form and as exactly compact as the more common form of saving the object's collection of transversal slices. Thus, memorizing 3-D objects from the beginning in the form of their angular projections can save a lot of computation later. Alternatively, one can avoid computing the set of angular projections if these projections are recorded by a camera from various viewpoints of a realistic object. Since the same algorithm can be applied for holograms of realistic 3-D scenes, the proposed process may replace part of the traditional holographic recording done by coherent beam interference. In comparison with the work described in section 2, the process is symmetric in both transverse axes. Therefore the volume effects exist in all transverse directions. The process is a reliable imitation of the Fourier holographic coherent system. Therefore, the reconstructed image has features similar to those of an image produced by a coherently recorded Fourier hologram. It should be mentioned that although the method is seemingly limited to Fourier holograms, once the complex wave front on the Fourier plane is computed, any other type of hologram, such as Fresnel or image holograms, can also be computed. This can be done simply by computing the propagation of the wave front from the Fourier plane to any other desired plane by means of Fresnel or near-field operators.

Possible applications of the suggested CGH are in areas where the 3-D representation is required. Areas such as computer-aided design, computer graphics, virtual reality, 3-D work stations, tomography, and holographic cameras might benefit from the proposed method. Since our hologram is classified as a Fourier hologram, it can also be applied to the areas of object recognition and target tracking in 3-D space.[33]

ACKNOWLEDGMENT

This research was supported by the Israel Science Foundation, grant 119/03.

REFRENCES

1. T. Inoue and H. Ohzu, "Accommodative responses to stereoscopic three-dimensional display," Appl. Opt. **36**, pp. 4509-4515, 1997.
2. K. Langhans, D. Bezecny, D. Homann, C. Vogt, C. Blohm, and K-H. Scharschmidt, "New portable FELIX 3-D display," Proc. SPIE **3296**, pp. 204-216 1998.
3. S. W. Min, Jung, J. H. Park, and B. Lee, "Three-dimensional display system based on computer-generated integral photography," Proc. SPIE **4297**, pp. 187-195, 2001.
4. S. A. Benton, "Holographic displays: 1975-1980," Opt. Eng. **19**, pp. 686-696, 1980.
5. D. Gabor, "A new microscope principle," Nature **161**, p. 777, 1948.
6. D. J. DeBitetto, "Holographic panoramic stereograms synthesized from white light recordings," Appl. Opt. **8,** pp. 1740-1741, 1969.
7. P. Hariharan, *Optical Holography* 2nd ed. Ch. 8, p. 139, Cambridge New York, 1996.
8. H. J. Caulfield, *Handbook of Optical Holography* Ch. 5, p. 211, Academic Press New York, 1979.

9. J. W. Goodman, *Introduction to Fourier Optics*, 2nd ed. Ch. 9, p. 326, Mcgraw-Hill New York, 1996.
10. E. N. Leith, and J. Upatnieks, "Wavefront reconstruction with diffused illumination and three-dimensional objects," J. Opt. Soc. Am., **54**, 1295, 1964.
11. A. W. Lohmann and D. P. Paris, "Binary Fraunhofer holograms generated by computer," Appl. Opt. **6,** pp. 1739–1748, 1967.
12. O. Bryngdahl and F. Wyrowski, "Digital holography-computer-generated holograms," in *Progress in Optics*, E. Wolf, ed. **28**, pp. 1-86, North-Holland, Amsterdam, 1990.
13. P. Hariharan, *Optical Holography*, 2nd ed. Ch. 10, p. 163, Cambridge, New York, 1996.
14. J. P. Waters, "Holographic image synthesis utilizing theoretical methods," Appl. Phys. Lett. **9**, pp. 405-407, 1966.
15. Y. Ichioka, M. Izumi, and T. Suzuki, "Scanning halftone plotter and computer-generated continuous tone hologram", Appl. Opt. **10**, pp. 403-411, 1971.
16. T. Yatagai, "Stereoscopic approach to 3-D display using computer-generated holograms," Appl. Opt. **15,** pp. 2722-2729, 1976.
17. N. George and J. T. McCrickerd, "Holography and stereoscopy: the holographic stereogram," SPIE **13**, pp. 342-350, 1969.
18. L. P. Yaroslavskii and N. S. Merzlyakov, *Methods of Digital Holography*, Consultants Bureau Plenum, New York, 1980.
19. C. Frère, D. Leseberg, and O. Bryngdahl, "Computer-generated holograms of 3-D objects composed of line segments," J. Opt. Soc. Am. A 3, pp. 726-730, 1986.
20. D. Leseberg and C. Frère, "Computer-generated holograms of 3-D objects composed of tilted planar segments," Appl. Opt. **27**, pp. 3020-3024, 1988.
21. T. Tommasi and B. Bianco, "Computer-generated holograms of tilted planes by spatial-frequency approach, "J. Opt. Soc. Am. A **10**, pp. 299-305, 1993.
22. M. Lucente, *Diffraction Specific fringe computation for electro-holography*, Doctoral Thesis Dissertation, MIT Dept of Electrical Engineering and computer Science, 1994.
23. C. D. Cameron, D. A. Pain, M. Stanley and C. W. Slinger, "Computational challenges of emerging novel true 3-D holographic displays," SPIE **4109,** pp. 129-140, 2000.
24. Y. Li, D. Abookasis, and J. Rosen, "Computer-generated holograms of three-dimensional realistic objects recorded without wave interference," Appl. Opt. **40**, pp. 2864-2870, 2001.
25. D. Abookasis and J. Rosen, "Computer-generated holograms of three-dimensional objects synthesized from their multiple angular viewpoints," J. Opt. Soc. Am. A **20**, pp. 1537-1545, 2003.
26. J. Rosen, "Three-dimensional joint transform correlator," Appl. Opt. **37,** pp. 7538-7544, 1998.
27. J. Rosen, B. Salik, A. Yariv and H.-K. Liu, "Pseudonondiffracting slit-like beam and its analogy to the pseudonondispersing pulse," Opt. Lett. **20**, pp. 423-425, 1995.
28. O. Bryngdahl and F. Wyrowski, "Digital holography - computer-generated Holograms," Prog. In Optics, E. Wolf, ed. **28**, pp. 1-86, North Holland, Amsterdam, 1990.
29. B. Salik, J. Rosen, and A. Yariv, "One-dimensional beam shaping," J. Opt. Soc. Am. A **12**, pp. 1702-1706, 1995.
30. A. B. VanderLugt, "Signal detection by complex spatial filtering," IEEE Trans. Inf. Theory IT-10, pp. 139–145, 1964.
31. S. Savchenko, *3-D Graphics Programming: Theory and Practice of Computer Graphics*, Ch. 2, pp. 46-53, SAMS Press, 2001.
32. J. J. Burch, "A computer algorithm for the synthesis of spatial frequency filter," Proc. IEEE **55**, pp. 599-601, 1967.
33. Y. Li and J. Rosen, "Object recognition using three-dimensional optical quasi-correlation," J. Opt. Soc. Am. A **19**, pp. 1755-1762, 2002.